\$ SUPER

Contents lists available at ScienceDirect

Bioresource Technology

journal homepage: www.elsevier.com/locate/biortech





Rational spatial rewiring of key enzymes enhances α -santalene production in *Saccharomyces cerevisiae*

Wenwen Tan ^{a,b,1}, Shengkun Tong ^{b,1}, Yaojie Gao ^b, Jing Wang ^a, Jingyu Zhang ^{a,c}, Zhiping Xie ^b, Huanqin Dai ^{d,e}, Yu Liang ^{a,b}, Gao-Yi Tan ^a, Lixin Zhang ^{a,c,*}, Yaojun Tong ^{b,*}

- a State Key Laboratory of Bioreactor Engineering, School of Biotechnology, East China University of Science and Technology, Shanghai 200237, China
- ^b State Key Laboratory of Microbial Metabolism, Joint International Research Laboratory of Metabolic and Developmental Sciences, School of Life Sciences and Biotechnology, Shanghai Jiao Tong University, Shanghai 200240, China
- ^c Shanghai Collaborative Innovation Center for Biomanufacturing Technology (SCIBT), Shanghai 200237, China
- d State Key Laboratory of Mycology, Institute of Microbiology, Chinese Academy of Sciences, Beijing, China
- ^e Medical School, University of Chinese Academy of Sciences, Beijing 100049, China

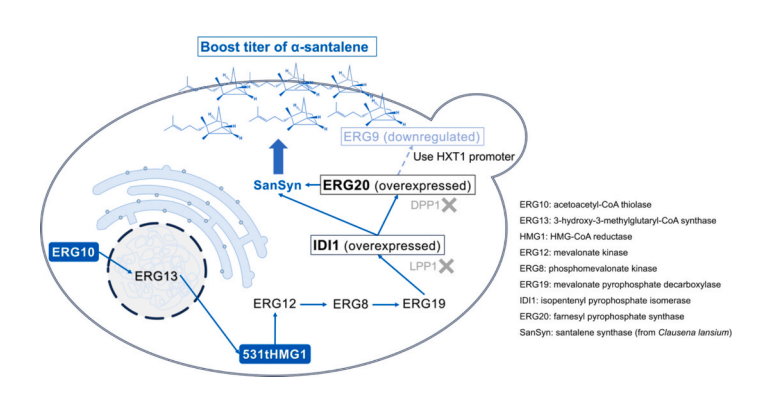
HIGHLIGHTS

- ullet Systematic subcellular mapping identifies bottlenecks limiting lpha-santalene biosynthesis in yeast.
- Comparative analysis of enzyme variants uncovers critical structure–function relationships affecting pathway performance.
- $\begin{tabular}{lll} \bullet & Multi-layered & metabolic & engineering \\ strategies & achieve & industrial-level \\ α-santalene & titers & in & fed-batch \\ fermentation. \\ \end{tabular}$
- Establishes a broadly applicable platform for spatial metabolic pathway optimization and precision design in yeast.

ARTICLE INFO

Keywords:
Subcellular enzyme localization
Spatial engineering
«-Santalene
Saccharomyces cerevisiae
Metabolic engineering
Synthetic biology

GRAPHICAL ABSTRACTS



ABSTRACT

Spatial compartmentalization in eukaryotic cell factories often constrains the efficiency of metabolic pathways. Here, we systematically mapped the subcellular localization of nine core enzymes in the α -santalene biosynthetic pathway of *Saccharomyces cerevisiae*, identifying metabolic bottlenecks associated with nuclear and endoplasmic reticulum (ER) localization. Through rational spatial engineering, including bioinformatically guided HMG1 truncation to achieve ER release and nuclear export signal (NES) tagging of key enzymes, we successfully rewired enzyme localization to enhance pathway flux. Coupled with promoter engineering to downregulate ERG9, addition-copy integration for IDI1 and ERG20 overexpression, and targeted medium optimization to improve cellular osmotolerance, we achieved substantial synergistic effects on production, leading to a 132-fold increase in α -santalene titer, reaching 568.59 mg/L in fed-batch fermentation. Our results demonstrate that combining subcellular localization engineering with classic metabolic and process optimization offers a robust and

https://doi.org/10.1016/j.biortech.2025.133027

^{*} Corresponding authors at: State Key Laboratory of Bioreactor Engineering, School of Biotechnology, East China University of Science and Technology, Shanghai 200237, China (L. Zhang).

E-mail addresses: lxzhang@ecust.edu.cn (L. Zhang), yaojun.tong@sjtu.edu.cn (Y. Tong).

 $^{^{1}}$ These authors contributed equally to this work and should be regarded as co-first authors.

generalizable strategy for high-level terpenoid biosynthesis in *S. cerevisiae*. This approach not only advances the performance of *S. cerevisiae* cell factories but also holds promise for broader application across other yeast species and eukaryotic microbial hosts.

1. Introduction

Terpenoids are structurally diverse isoprene-derived natural products that possess potent biological activities, including anti-cancer, antiinflammatory, and antimicrobial effects, rendering them valuable in pharmaceutical, cosmetic, and food industries (Chen et al., 2024; Hong & Nielsen, 2012). Among these, α-santalene, a sesquiterpene and major component of sandalwood essential oil (Yan et al., 2024), exhibits notable therapeutic properties such as anti-tumor, anti-inflammatory, and antibacterial activities (Adams et al., 1975). Through monooxygenation, α -santalene can be converted into α -santalol, the principal bioactive compound of sandalwood oil, which holds significant commercial interest (Bommareddy et al., 2019; Celedon et al., 2016). Traditionally, sandalwood essential oil is obtained through steam distillation of heartwood and roots from Santalum album (Burdock & Carabin, 2008). However, the slow growth, stringent ecological requirements, and overexploitation of sandalwood trees, exacerbated by climate change, severely constrain its supply and sustainability (Zhang et al., 2017). Thus, developing alternative, renewable production strategies is urgently required.

Microbial cell factories offer a promising alternative due to their fast growth, small ecological footprint, and genetic tractability (Kim et al., 2025). Recent advances in synthetic biology (Voigt, 2020) have facilitated the design and reconstruction of microbial metabolic pathways for the sustainable production of high-value natural products (Liu et al., 2024; Zhang et al., 2022). Among microbial hosts, Saccharomyces cerevisiae is widely used owing to its robust fermentation performance, comprehensive genetic toolbox, and Generally Recognized as Safe (GRAS) status (Ostergaard et al., 2000). Nonetheless, as a eukaryote, S. cerevisiae exhibits intrinsic subcellular compartmentalization, spatially separating metabolic enzymes across organelles such as the nucleus, endoplasmic reticulum (ER), cytoplasm, and mitochondria. This spatial separation will hinder substrate channeling and reduce overall metabolic efficiency (Wang & Li, 2017). Emerging evidence suggests that reducing spatial separation between pathway enzymes can significantly enhance metabolic flux and overall product titers (Geraldi et al., 2021). Targeting enzymes to specific organelles, such as mitochondria or peroxisomes, not only facilitates substrate channeling but can also mitigate cytotoxicity and further boost production yields (Avalos et al., 2013; Awan et al., 2017; Kulagina et al., 2021; Song et al., 2024; Zhang et al., 2023). For example, localization of the geraniol biosynthesis pathway to peroxisomes via the PST1 targeting signal in Pichia pastoris increased geraniol titers by more than 30 % compared to cytosolic localization (Ye et al., 2024). Therefore, accurate protein localization is crucial for optimizing heterologous pathways in synthetic biology applications, as mis-localized enzymes may suffer reduced activity or impaired stability (Awan et al., 2017; Grewal et al., 2021; Liu et al., 2024; Ye et al., 2024).

Microbial production of α -santalene and its oxidized derivative α -santalol has been pursued primarily by introducing α -santalene synthase (SanSyn) into *S. cerevisiae*, coupled with enhancement of the mevalonate (MVA) pathway and downregulation of ERG9 to redirect FPP flux toward sesquiterpene biosynthesis (Scalcinati et al., 2012a; Scalcinati et al., 2012c; Zuo et al., 2022). Additional strategies, including biphasic fermentation and cytochrome P450 (e.g., CYP736A167)-mediated α -santalol synthesis, have further improved yields (Tippmann et al., 2016a; Zha et al., 2020). However, the majority of previous efforts have focused on pathway reconstruction and metabolic flux optimization, with limited consideration of enzyme subcellular localization. To date, there have been no systematic studies

integrating localization engineering with genome-level pathway design for α -santalene biosynthesis in yeast.

In this study, we systematically characterized the subcellular localization of nine enzymes in the α-santalene biosynthetic pathway in S. cerevisiae, identifying localization-based metabolic bottlenecks. Guided by bioinformatic predictions, we rationally designed truncated enzyme variants, notably HMG1, to improve cytoplasmic accessibility and metabolic flux. Our experiments highlight that not all literaturederived enzyme variants work as expected and must be empirically tested in the specific metabolic context.. By applying targeted spatial reprogramming strategies, including nuclear export signal (NES) tagging and enzyme truncation, coupled with gene overexpression, promoter optimization, and fermentation condition refinement, we substantially improved α -santalene production. Ultimately, a 5L-fedbatch fermentation confirmed the scalability of our engineered strain, achieving an industrially relevant titer of 568.59 mg/L, and demonstrating the broad applicability and effectiveness of spatial metabolic engineering in microbial production of high-value terpenoids.

2. Materials and methods

2.1. Strains, media, and cultivation conditions

Escherichia coli DH5α was used for plasmid construction and propagation, cultured in LB medium (10 g/L tryptone, 5 g/L yeast extract, 10 g/L NaCl, 20 g/L agar was added for solidification when needed) supplemented with 100 mg/L ampicillin at 37 °C, 220 rpm. Saccharomyces cerevisiae BY4742 was cultivated in YPD medium (10 g/L yeast extract, 20 g/L glucose, 20 g/L Peptone, 20 g/L agar was added for solidification) at 30 °C, 220 rpm. For selection, SD dropout plates (SD-Uracil, SD-Leucine, SD-Histidine, and SD-Lysine) were used (6.7 g/L yeast nitrogen base without amino acids, 20 g/L glucose, 20 g/L agar, supplemented with amino acids except for the corresponding dropout: uracil 40 mg/L, lysine 30 mg/L, adenine 30 mg/L, methionine 30 mg/L, histidine 40 mg/L, leucine 100 mg/L, and tryptophan 100 mg/L). YPD-Gal medium consisted of 10 g/L yeast extract, 2 g/L glucose, 18 g/L galactose, and 20 g/L peptone. SMD medium contained 6.7 g/L yeast nitrogen base without amino acids, 20 g/L glucose, 15 g/L agar, and the same amino acids supplementation as above. The fermentation medium contained 10 g/L yeast extract, 20 g/L peptone, 5 g/L ammonium sulfate, 20 g/L galactose, 10 g/L glucose, and 2.5 mM betaine. The feed medium consisted of 10 g/L yeast extract, 20 g/L peptone, 5 g/L ammonium sulfate, and 200 g/L glucose.

2.2. Plasmids construction

High-fidelity PCR amplification was performed using the Q5® High-Fidelity 2 × Master Mix (New England Biolabs). Yeast genes were amplified from *S. cerevisiae* BY4742 genomic DNA, and PCR products were purified using the FastPure Gel DNA Extraction Mini Kit (Vazyme). All heterologous genes were synthesized by GenScript. Plasmids including pBS406-ERG8-GFP, pBS406-ERG10-GFP, pBS406-ERG12-GFP, pBS406-ERG20-GFP, pBS406-IDI1-GFP, pBS406-HMG1-GFP, and pBS405-GAL1-SanSyn-GFP-tADH1 were constructed using the Golden Gate assembly method (Engler et al., 2008). All other plasmids were assembled via the Gibson assembly approach (Gibson, 2011). Golden gate and Gibson assemblies were performed using the NEBridge® Golden Gate Assembly Kit (*Bsa*I-HF® v2, NEB) and the ClonExpress Ultra One Step Cloning Kit (Vazyme), respectively. Recombinant plasmids were transformed into *E. coli* DH5α, validated by PCR and Sanger

sequencing. The confirmed correct constructs were stored at -80 °C.

2.3. Strains construction using CRISPR-Cas9 or homologous recombination

Engineered S. cerevisiae strains were constructed using either CRISPR-Cas9 genome editing system (DiCarlo et al., 2013) or homologous recombination (Rothstein, 1991). Yeast transformation were carried out using the lithium acetate/single-stranded DNA protocol (Gietz & Schiestl, 2007). Positive transformants were selected on appropriate dropout media or antibiotic-containing media. Plasmids for subcellular localization were constructed by fusing a S. cerevisiae codon-optimized GFP gene to the C-terminus of each target enzyme via a flexible GGGS linker. Linearized plasmids were integrated into the S. cerevisiae BY4742 genome at the promoter region by homologous recombination. For CRISPR-Cas9-based protocol, the plasmid pCas9 + delta-gRNA and linearized donor DNA were co-transformed into S. cerevisiae cells and plated onto selective media for antibiotic resistance or auxotrophy complementation. The spacer for sgRNA construct was designed using Benchling. To eliminate the pCas9 + delta-gRNA plasmid, transformants were cultured in liquid YPD medium for 12 h, serially diluted, and plated. Single colonies were picked into 10 uL sterile ddH₂O, and 1–2 uL were spotted onto URA-selective plates. Colonies that failed to grow on URA selection were considered to have successfully lost the pCas9 +

To construct production strains, cassettes S0 to S4 were cotransformed with pCas9 \pm delta-gRNA into BY4742 to generate the engineered strains SBYS0, SBYS1, SBYS2, SBYS3, and SBYS4. Subsequently, cassettes A1 and A2 were introduced into SBYS3 and SBYS4, yielding strains SBYS3-A1, SBYS3-A2, SBYS4-A1, and SBYS4-A2 via homologous recombination. Further transformation of cassettes B1 and B2 into SBYS4-A1 and SBYS4-A2 led to the construction of strains SBYS4-A1-B1, SBYS4-A1-B2, SBYS4-A2-B1, and SBYS4-A2-B2. Finally, the R cassette was independently integrated into each of these strains, resulting in the final engineered strains: SBYS4-A1-B1-R, SBYS4-A1-B2-R, SBYS4-A2-B1-R, and SBYS4-A2-B2-R.

2.4. Fluorescence microscopy and image processing

A single *S. cerevisiae* colony was inoculated into 8 mL YPD (or YPD-Gal for strains requiring galactose) and incubated overnight at 30 °C, 220 rpm. The overnight culture was diluted to an initial OD600 of approximately 0.2 and regrown to OD600 \approx 0.7. Subsequently, 2 mL of culture was harvested by centrifugation at 5000 rpm for 2 min and resuspended in 2 mL of SMD medium. A 300 μ L aliquot of the cell suspension was applied to a Concanavalin A (ConA)-coated coverslip and incubated for 5 min to facilitate cell attachment. Fluorescence imaging was performed using an OLYMPUS IX83 fully automated fluorescence microscope, and images were processed using ImageJ (Version 1.54 k) (Schneider et al., 2012).

2.5. Yeast flask cultivation and α -santalene extraction

Positive transformants were inoculated into 5 mL YPD and cultured for 24 h at 30 °C, 200 rpm. 1 mL aliquot was transferred to 50 mL YPD-Gal medium in a 250 mL shake flask and incubated for 24 h under the same conditions. Then 10 % (v/v) n-dodecane (5 mL) was added, and fermentation was continued for 3–4 days. Post-fermentation, 10 mL culture was centrifuged for 5 min at 5000 rpm, room temperature, and the n-dodecane layer was extracted, diluted with n-hexane, dehydrated with Na₂SO₄, filtered through a 0.22 μ m nylon membrane, and analyzed via GC–MS.

2.6. GC-MS quantification

An Agilent GC-7890B coupled with MS-5977B and HP-5MS capillary

column was used in selected ion monitoring (SIM) mode. Conditions: injection temp 250 °C, ion source 250 °C, electron energy 70 eV, solvent delay 10 min. The oven program: 40 °C (3 min), ramp to 130 °C at 10 °C/min, then to 180 °C at 2 °C/min, then to 300 °C at 50 °C/min, hold for 10 min. Mass range: m/z 40–500; SIM ions: 93, 94, 105, 107, 119, 122, 202. Quantification of α -santalene using β -caryophyllene as external standard.

2.7. Standard curve

 β -Caryophyllene (4 mg) was dissolved in *n*-hexane to prepare a 10 mL stock solution (400 mg/L). The stock was serially diluted to prepare standards at 100, 50, 25, 5, and 1 mg/L. GC–MS analysis was used for quantification, and chromatographic areas were integrated to generate a standard curve.

2.8. Fed-batch fermentation

A single colony was first inoculated into 10 mL YPD medium and cultivated at 30 °C with shaking at 220 rpm for 24 h. Two seed cultures were then combined to inoculate 200 mL of fermentation medium in a 1-L flask (at 10 % v/v inoculation). After an additional 24-h incubation under the same conditions, the entire culture was transferred to a 5-L fermenter containing 2 L fresh fermentation medium. The fermentation was carried out at 30 °C with pH maintained between 5.0 and 5.5 using NH₄OH for automatic adjustment. Dissolved oxygen (DO) was controlled at 30 % by adjusting the agitation speed (300–450 rpm), with an aeration rate of 2-3 L/min. Both glucose concentration and cell density (OD600) were monitored periodically. After 24 h of batch cultivation, a continuous glucose feeding strategy was initiated, with the feed rate dynamically adjusted based on real-time residual glucose measurements to maintain low glucose levels and avoid ethanol accumulation. At 48 h, galactose (60 g) was added to induce expression of GAL promoters, together with 250 mL of n-dodecane as an in situ extractant, and glucose feeding was terminated. Fermentation was continued to 144 h. Samples from the organic phase were collected at designated time points, centrifuged to remove cell debris, and diluted in n-hexane prior to analysis. α -santalene concentrations were determined by GC-MS.

2.9. RNA extraction and RT-qPCR

Yeast cells were cultured and induced under the same conditions as flask fermentation. Total RNA was extracted using the Spin Column Yeast Total RNA Purification Kit (Sangon), including an on-column DNase I digestion step (Vazyme) to remove genomic DNA. RNA concentration was determined using a NanoDrop 2000 spectrophotometer (Thermo Fisher Scientific), and RNA integrity was verified by agarose gel electrophoresis. cDNA synthesis and quantitative PCR were performed using ToloScript All-in-one RT EasyMix (ToloBio) and TB Green Premix Ex Taq II (Takara), respectively, following the manufacturers' protocols. ACT1 served as the reference gene. Relative mRNA levels were calculated using the $2^{-\Delta\Delta Ct}$ method (Livak & Schmittgen, 2001).

2.10. Statistical analysis

All experiments were performed with at least three independent biological replicates. Statistical significance was evaluated using one-way analysis of variance (ANOVA) followed by Tukey's honestly significant difference (HSD) test for multiple comparisons, unless otherwise specified. For comparisons involving multiple groups against a single control (e.g., different supplementation conditions vs. 0 mM or 0 g/L), Dunnett's multiple comparisons test was applied. A p-value of less than 0.05 was considered statistically significant. Significance levels are indicated as follows: p < 0.05 (*), p < 0.01 (***), p < 0.001 (***). Statistical analyses were conducted using GraphPad Prism 10.0.

3. Results

3.1. Subcellular localization profiling of key enzymes in the α -santalene biosynthesis pathway

α-Santalene is synthesized via the cyclization of farnesyl pyrophosphate (FPP), a 15-carbon intermediate derived from the mevalonate (MVA) pathway in S. cerevisiae. In this pathway, one molecule of dimethylallyl diphosphate (DMAPP) and two molecules of isopentenyl diphosphate (IPP) are condensed sequentially to form FPP, the direct precursor of sesquiterpenes (Fig. 1A). FPP can be converted to α -santalene by the santalene synthase. To initiate heterologous production of α-santalene in S. cerevisiae BY4742, we used CRISPR-Cas9-based genome editing approach (DiCarlo et al., 2013) to integrate the Clausena lansium santalene synthase gene (SanSyn) (Schalk, 2013) into its genome (Fig. 1B) under the control of the galactose-inducible GAL1 promoter at the δ-site, resulting in a baseline strain SBYS0 (Unless otherwise specified, all yield comparisons in this study were performed using SBYSO as the reference group), which produced 4.29 mg/L α-santalene upon galactose induction (Fig. 1C). To systematically enhance α -santalene production, we innovated key enzyme re-localization combining with a modular metabolic engineering strategy of gene overexpression, flux redirection, medium refinement, and scale-up fermentation.

Given that subcellular localization critically influences metabolic flux, we first systematically mapped the subcellular distribution of nine key enzymes within the α -santalene biosynthetic pathway using GFP-tagged proteins visualized by fluorescence microscopy. Localization patterns were assigned based on comparisons with organelle-specific markers (Zhu et al., 2019).

As shown in Fig. 2A, enzymes ERG8, ERG12, ERG19, ERG20, IDI1, and SanSyn were predominantly localized to the cytoplasm, whereas

ERG10 and ERG13 were notably confined to the nucleus. Notably, the rate-limiting enzyme HMG1 (Bröker et al., 2018; Meng et al., 2020), displayed ER membrane localization, suggesting potential accessibility constraints and flux limitations through the ER membrane barrier.

3.2. Rational design and spatial reprogramming of HMG1

To address this, we designed a truncated HMG1 variant to re-localize the enzyme to the cytoplasm. Using transmembrane domain prediction software (TMHMM-2.0) (Moller et al., 2001), we identified amino acid 522 as a potential truncation site to yield a cytoplasmic variant, termed 522tHMG1 (Fig. S2A and S2C). GFP-fusion microscopy validated successful relocalization to the cytoplasm (Fig. 2B). Although strain SBYS2 (expressing 522tHMG1) (Fig. 3A) showed an improved α-santalene yield (14.52 mg/L) (Fig. 3B), this improvement was modest, indicating the necessity of experimental validation. Further evaluation using an alternative prediction algorithm (DeepTMHMM) (Hallgren et al., 2022) indicated minor discrepancies in truncation points (position 520 vs. 522), showing the inherent uncertainty. We then tested the only two literature-reported truncated variants, 531tHMG1 (Polakowski et al., 1998) and AA531tHMG1 (Donald et al., 1997). Remarkably, the strain expressing 531tHMG1 (SBYS4) achieved significantly higher productivity (26.05 mg/L), demonstrating that subtle amino acid differences can critically impact catalytic performance (Fig. 3B). These findings not only align with previous reports (Meng et al., 2020; Polakowski et al., 1998) but also reveal the complexity and context-dependency of enzyme truncation and emphasize the value of empirical verification.

The superior performance of the 531tHMG1 variant aligns with previous reports where cytosolic expression of HMG1 boosted metabolic flux (Polakowski et al., 1998). Importantly, our initial attempt with 522tHMG1 highlights the importance of experimental validation of

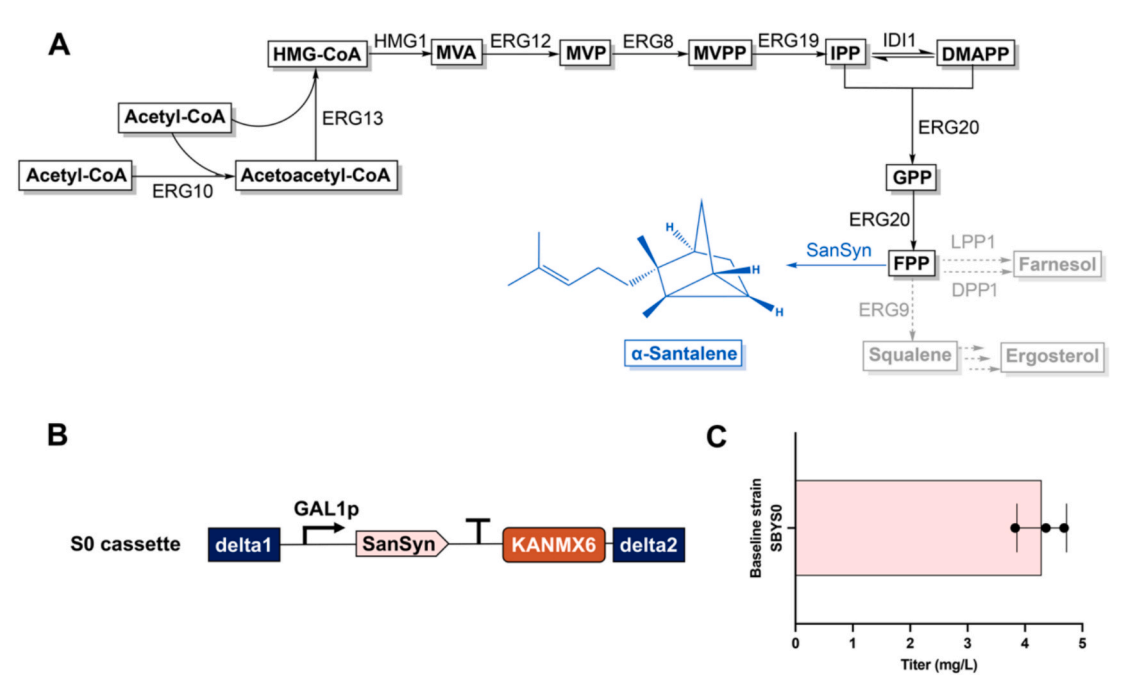


Fig. 1. Heterologous biosynthetic pathway of α-santalene in S. cerevisiae and baseline strain construction. A. Schematic of the α-santalene biosynthetic pathway in S. cerevisiae. Key enzymes: ERG10, acetoacetyl-CoA thiolase; ERG13, 3-hydroxy-3-methylglutaryl-CoA synthase; HMG1, HMG-CoA reductase; ERG12, mevalonate kinase; ERG8, phosphomevalonate kinase; ERG19, mevalonate pyrophosphate decarboxylase; IDI1, isopentenyl pyrophosphate isomerase; ERG20, farnesyl pyrophosphate synthase; SanSyn, santalene synthase (from Clausena lansium (Schalk, 2013)); ERG9, squalene synthase. Intermediate metabolites: MVA, mevalonate; MVP, mevalonate-5-phosphate; MVPP, mevalonate-5-pyrophosphate; IPP, isopentenyl pyrophosphate; DMAPP, dimethylallyl pyrophosphate; GPP, geranyl pyrophosphate; FPP, farnesyl pyrophosphate. Dotted arrows indicate competing branches leading to farnesol and sterol biosynthesis via LPP1 (diacylglycerol pyrophosphate phosphatase), and ERG9 (squalene synthase), respectively. Integration strategies targeting LPP1 and DPP1 loci are shown in subsequent figures to further channel FPP toward α-santalene production. B. Structure of the S0 cassette used for heterologous expression of SanSyn, integrated at the δ loci under the control of the GAL1 promoter. C. Baseline α-santalene titer of strain SBYS0 under shake flask conditions. Data represent mean \pm standard deviation (n = 3 biological replicates).

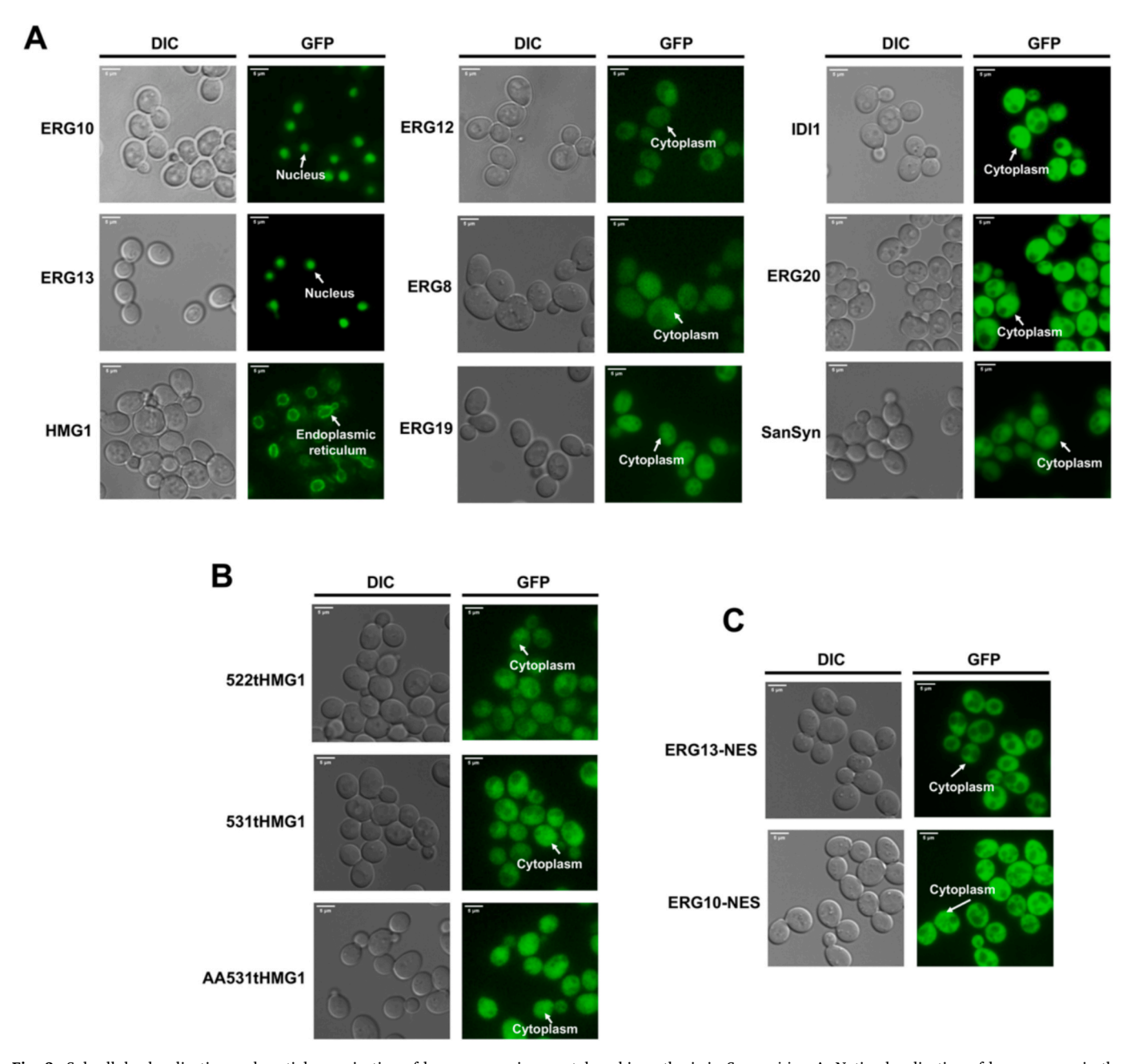


Fig. 2. Subcellular localization and spatial organization of key enzymes in α -santalene biosynthesis in S. cerevisiae. A. Native localization of key enzymes in the α -santalene biosynthetic pathway, including ERG10, ERG13, HMG1, ERG12, ERG8, ERG19, IDI1, ERG20, and SanSyn. Enzymes were distributed across distinct cellular compartments including the nucleus, cytoplasm, and ER. B. Subcellular localization of three truncated variants of HMG1. C. Re-localization of ERG10 and ERG13 using C-terminal fusion to a NES. NES-tagged proteins were successfully redirected from the nucleus to the cytoplasm. All subcellular localizations were visualized using GFP fusions.

bioinformatic predictions and shows that literature-derived variants may not always translate directly to different metabolic contexts.

3.3. Spatial rewiring ERG13 combined with co-overexpressing IDI1 and DPP1 disruption enhance α -santalene titer

Following successful HMG1 relocalization, we further investigated whether the re-localization of the two nuclear-localized enzymes ERG13 and ERG10 to the cytoplasm could further enhance the metabolic flux of MVA pathway. We fused each enzyme to a nuclear export signal (NES) derived from yeast Nmd3 (Gadal et al., 2001), and subcellular relocalization was confirmed by fluorescence microscopy (Fig. 2C). Building upon the two good-performing strains (SBYS3 and SBYS4)

carrying truncated variants of HMG1, we constructed additional expression cassettes enabling co-overexpression of IDI1 and either native ERG13 or ERG13-NES. These cassettes were genomically integrated at the DPP1 locus, a diacylglycerol pyrophosphate phosphatase, such that locus disruption reduced competing FPP hydrolysis (Fig. 4A). As confirmed by RT-qPCR, the relative mRNA levels of IDI1 in both SBYS4-A1 and SBYS4-A2 were over 10-fold higher than in the parental strain SBYS4 (Fig. 4C). Functionally, co-overexpression of IDI1 and cytoplasmic ERG13-NES with 531tHMG1 (strain SBYS4-A2) significantly elevated α -santalene titer to 56.16 mg/L, almost double that of its native ERG13 counterpart strain SBYS4-A1 (Fig. 4B). Similar trends were observed in SBYS3 background strains, albeit with overall lower titers compared to SBYS4 derivatives. These results indicate the

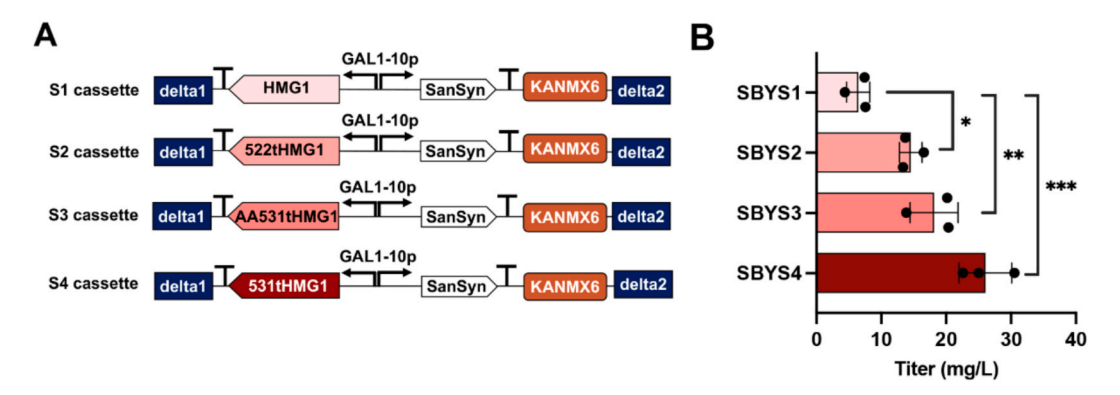


Fig. 3. Rational design and functional evaluation of HMG1 truncation variants for enhanced α-santalene biosynthesis. A. Schematic of engineered cassettes for co-expression of HMG1 (full-length or truncated) and santalene synthase under the GAL1-10 promoter, integrated at the δ loci in the yeast genome. The truncation variants include 522tHMG1, AA531tHMG1, and 531tHMG1 with S1-S4 cassettes corresponding to full-length HMG1, 522tHMG1, AA531tHMG1, and 531tHMG1, respectively. All constructs contain the KANMX6 marker for selection and were PCR-amplified from plasmid templates. B. α-Santalene titers of engineered strains SBYS1-SBYS4 under shake flask conditions. Data represent mean \pm standard deviation (n = 3 biological replicates). Statistical significance between groups was assessed using one-way ANOVA followed by Tukey's HSD test. Significance levels are indicated as follows: p < 0.05 (*), p < 0.01 (**), p < 0.001 (***).

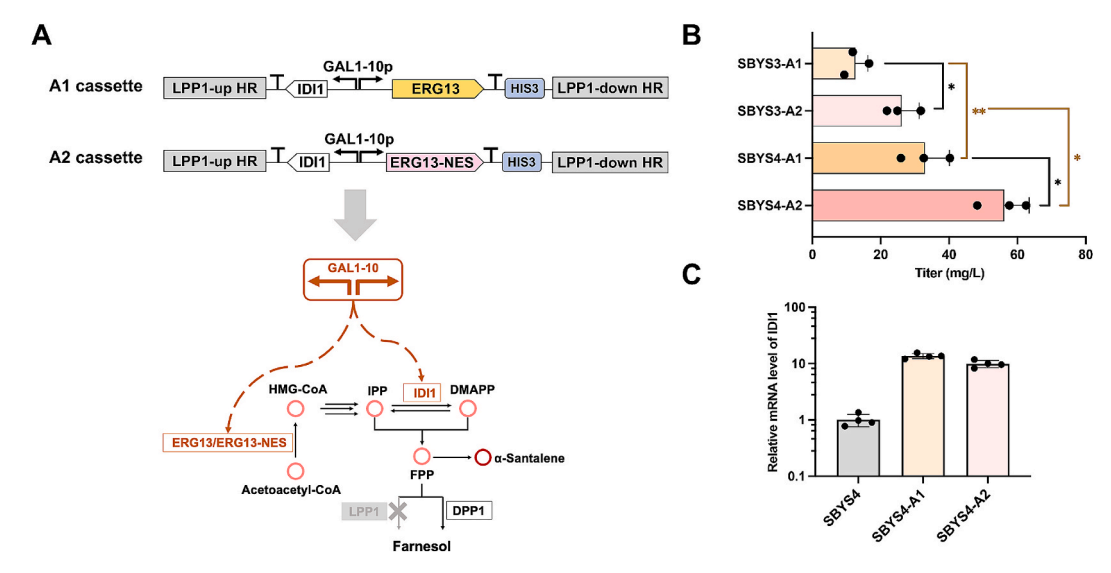


Fig. 4. Spatial reprogramming of ERG13 and addition-copy IDI1 expression at the LPP1 locus for enhanced α-santalene production. A. Schematic of A1 and A2 expression cassettes used for genomic integration at the LPP1 locus. Cassette A1 enables co-expression of IDI1 and native ERG13 under the bidirectional GAL1-10 promoter, while cassette A2 co-expresses IDI1 and the cytosolic ERG13-NES variant. Both constructs are flanked by homology arms targeting LPP1 for integration and carry the HIS3 selection marker. Disruption of LPP1, a diacylglycerol pyrophosphate phosphatase, not only facilitates additional copy integration but also reduces FPP hydrolysis and farnesol formation, thereby improving precursor availability for α-santalene biosynthesis. B. α-Santalene titers of engineered strains SBYS3-A1, SBYS3-A2, SBYS4-A1 and SBYS4-A2, each harboring different HMG1 variants and ERG13/IDI1 expression modules. C. Quantitative RT-qPCR analysis of IDI1 transcript levels in engineered strains. IDI1 mRNA abundance was over 10-fold higher in both SBYS4-A1 and SBYS4-A2 compared to the parental strain SBYS4, confirming successful additional copy integration and strong expression. Data represent mean \pm standard deviation (n \ge 3 biological replicates). Significance among groups was determined by one-way ANOVA with Tukey's post-hoc test. Significance levels are indicated as follows: p < 0.05 (*), p < 0.01 (**).

importance of both spatial enzyme coordination and strategic chromosomal integration for maximizing metabolic flux and product yield (Fig. 4B).

3.4. Spatial rewiring ERG10 with ERG20 overexpressing, LPP1 disruption and ERG9 downregulation further boost α -santalene titer

To further increase the supply of FPP, we introduced additional cassettes encoding ERG20 with either native ERG10 or ERG10-NES, integrated at the LPP1 locus, another diacylglycerol pyrophosphate phosphatase whose disruption likewise limited competitive FPP hydrolysis while permitting additional copy integration (Fig. 5A). Consistent with the design, RT-qPCR analysis confirmed that ERG20 mRNA levels were significantly increased over 15-fold in engineered strains (Fig. 5E). Surprisingly, overexpression of ERG20, in combination with spatially

rewired ERG10, did not immediately improve α -santalene titers and in some cases decreased production (Fig. 5B), likely due to enhanced FPP flux toward sterol biosynthesis via squalene synthase (ERG9).

To mitigate this competitive drain, we replaced the native *ERG9* promoter with a weaker, glucose-inducible promoter (pHXT1) (Lewis & Bisson, 1991), thereby attenuating ERG9 expression and limiting FPP conversion to squalene (Fig. 5C). RT-qPCR further confirmed that ERG9 transcript abundance was markedly reduced following promoter replacement (Fig. 5E). Notably, ERG20 overexpression proved crucial for effective flux redirection only after ERG9 promoter attenuation. This combinatorial approach in strain SBYS4-A1-B2-R (expressing ERG10-NES, native ERG13, truncated 531tHMG1, ERG20 overexpression, and pHXT1-driven ERG9) resulted in a dramatic increase in α -santalene titer to 199.41 mg/L, a nearly 50-fold improvement over the baseline strain SBYS0 (Fig. 1C, and Fig. 5D). Interestingly, optimal production was

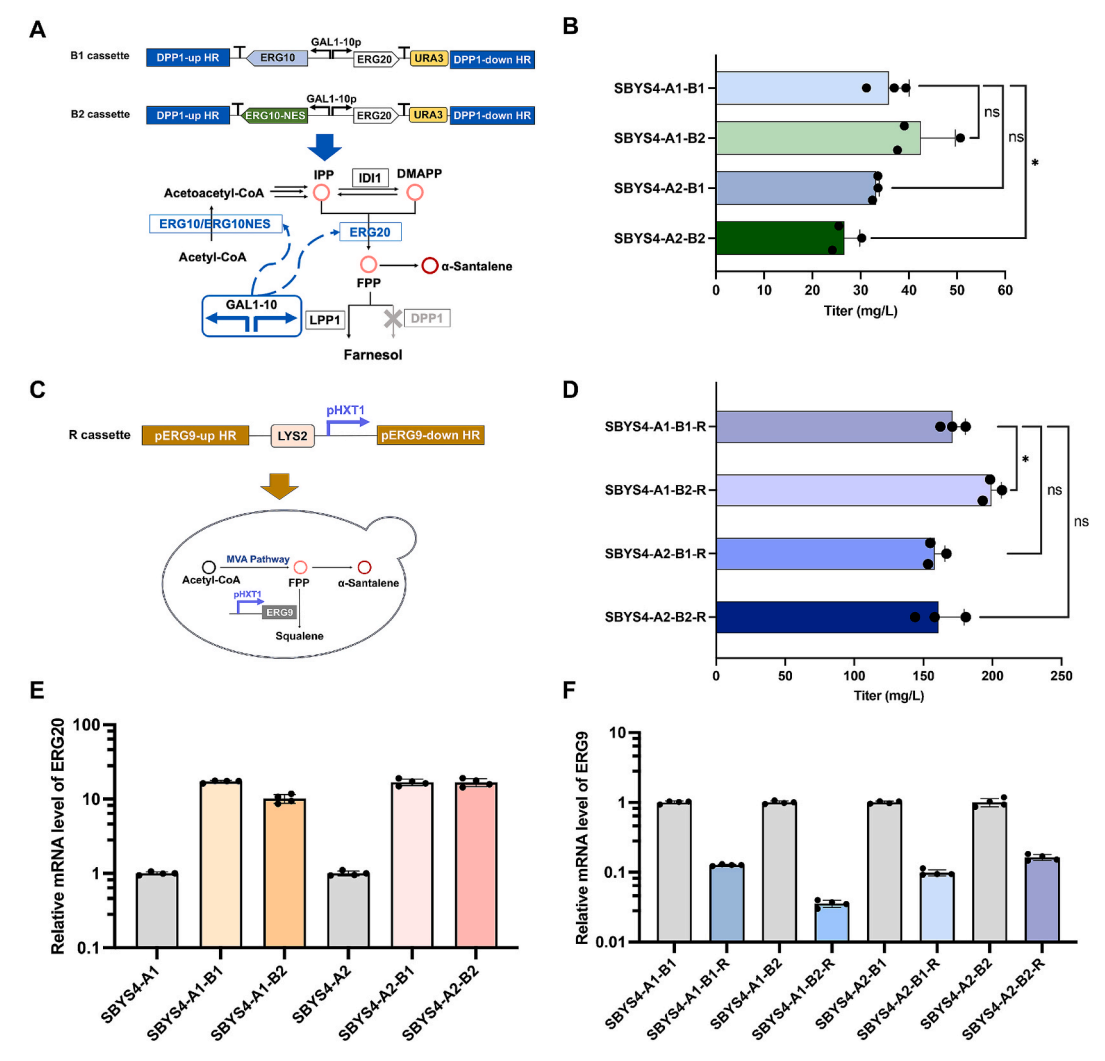


Fig. 5. Combinatorial spatial engineering of ERG10 and pathway rewiring via ERG20 overexpression and ERG9 downregulation to enhance α-santalene production. A. Schematic of B1 and B2 expression cassettes for genomic integration at the DPP1 locus. Cassette B1 enables co-expression of ERG20 and native ERG10 under the bidirectional GAL1-10 promoter, while cassette B2 contains ERG20 and cytosolic ERG10-NES. Both cassettes are flanked by DPP1 homology arms for targeted integration and carry the URA3 selection marker. Disruption of DPP1, a diacylglycerol pyrophosphate phosphatase, not only permits addition-copy integration but also reduces competitive FPP hydrolysis, channeling more flux toward α-santalene synthesis. B. α-Santalene titers of engineered strains SBYS4-A1-B1, SBYS4-A1-B2, SBYS4-A2-B1 and SBYS4-A2-B2, each harboring different spatial configurations of ERG10/ERG10-NES and ERG20 overexpression modules. C. Schematic of the R cassette used for promoter replacement of ERG9. The native ERG9 promoter was replaced with the weaker, glucose-inducible pHXT1 promoter, using a cassette flanked by homologous arms for targeted integration at the ERG9 locus. This modification downregulates ERG9 expression, reducing FPP diversion into sterol biosynthesis and further increasing precursor availability for α-santalene production. D. α-Santalene titers of engineered strains SBYS4-A1-B1-R, SBYS4-A1-B2-R, SBYS4-A2-B1-R and SBYS4-A2-B2-R, which combine different configurations of ERG10, ERG13, ERG20, and ERG9 regulation. E. Quantitative RT-qPCR analysis of ERG20 transcript levels in engineered strains. ERG20 mRNA levels were significantly increased in SBYS4-A1-B1, SBYS4-A1-B2, SBYS4-A2-B1, and SBYS4-A2-B2 compared to the parental strain SBYS4-A1 and SBYS4-A2, consistent with cassette-driven overexpression. F. Quantitative RT-qPCR analysis of ERG9 transcript levels in engineered strains. ERG9 mRNA abundance was markedly reduced in strains carrying the pHXT1-driven ERG9 promoter replacement (R cassette), confirming effective dow

achieved when ERG10 was localized to the cytoplasm and ERG13 remained in the nucleus, indicating a non-intuitive requirement for spatial enzyme partitioning to achieve balanced metabolic channeling.

3.5. Medium optimization and scale-up fermentation deliver industrially relevant titers

To further enhance $\alpha\text{-santalene}$ production, we optimized fermentation conditions of the best-performing SBYS4-A1-B2-R by evaluating medium supplements (for maintaining cell osmolality) and aeration methods. Initially, supplementation with glycerol (5 g/L and 10 g/L) and replacement of flask sealing film with gauze covers were tested. These changes yielded either negligible or modest improvements,

respectively (Fig. 6A). Subsequently, we tested betaine supplementation at five concentrations (1 mM, 2.5 mM, 5 mM, 10 mM, and 20 mM). The addition of 2.5 mM betaine notably increased α -santalene titers by 22 %, reaching 309.76 mg/L (Fig. 6B). Higher betaine concentrations were less beneficial, likely due to cytotoxicity or osmotic stress at elevated levels. These results suggest betaine as a practical additive for improving terpenoid production.

To validate scalability, fed-batch fermentation of strain SBYS4-A1-B2-R was conducted in a 5-L bioreactor. Initial glucose (10 g/L) and galactose (25 g/L) concentrations supported robust biomass accumulation. Glucose feeding initiated at 24 h and terminated at 48 h, coinciding with galactose addition (60 g) and dodecane overlay (250 mL) to induce α -santalene synthesis and facilitate *in situ* extraction. This optimized

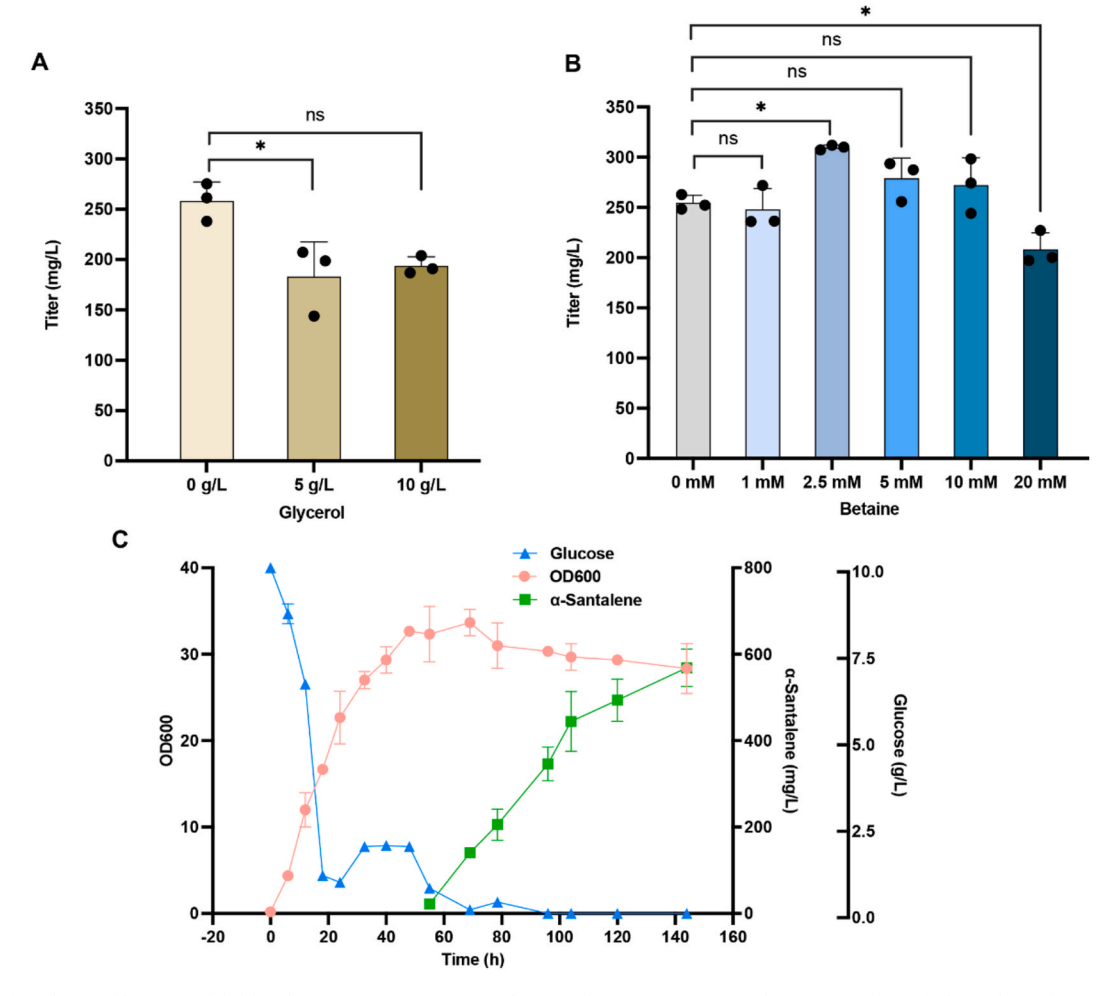


Fig. 6. Effects of medium additives and fed-batch fermentation on α-santalene production in engineered yeast. A. Effect of glycerol supplementation at different concentrations on α-santalene titer in strain SBYS4-A1-B2-R during shake flask fermentation. B. Effect of betaine supplementation at various concentrations on α-santalene titer in the same strain. C. Time-course profile of fed-batch fermentation in a 5-L bioreactor with the optimized strain SBYS4-A1-B2-R. A two-phase fermentation strategy was employed, with initial glucose feeding for biomass accumulation followed by galactose induction and n-dodecane overlay for in situ product extraction. The final α-santalene titer reached 568.59 mg/L. Data represent mean \pm standard deviation (n = 3 independent biological replicates). Statistical comparisons were performed using one-way ANOVA followed by Dunnett's test, with all groups compared to the 0 g/L or 0 mM control. Significance levels are indicated as follows: p < 0.05 (*).

process yielded a maximum α -santalene titer of 568.59 mg/L, an 84 % increase over shake flask cultivation (Fig. 6C and Fig. S1). These results showed the robustness and industrial potential of our engineered yeast platform for α -santalene production.

4. Discussion

Sesquiterpenes such as α -santalene and its oxidized derivative α -santalol are valuable compounds with extensive applications in pharmaceuticals, fragrances, and cosmetics. Due to the limited availability and sustainability issues associated with natural extraction from sandalwood trees, microbial biosynthesis presents an attractive alternative (Wang et al., 2021; Zha et al., 2020). Although α -santalene biosynthesis has been previously reconstituted in S. cerevisiae, achieving industrially relevant production titers remains challenging. In this study, we demonstrated a significant improvement in α -santalene biosynthesis through systematic enzyme localization engineering, gene expression optimization, flux redirection, and fermentation condition refinement.

Subcellular compartmentalization in eukaryotes, such as yeast, often restricts metabolic efficiency by physically separating pathway enzymes. Previous studies showed that minimizing spatial distances among enzymes can significantly improve metabolic flux and product

yields (Geraldi et al., 2021). Here, we revealed the native nuclear localization of ERG10 and ERG13 enzymes as a potential bottleneck in the early MVA pathway. Surprisingly, relocating both enzymes into the cytoplasm was not optimal; maximal α -santalene production required a balanced spatial arrangement, with ERG10 in the cytoplasm and ERG13 retained in the nucleus. This counterintuitive finding suggests that efficient channeling of acetoacetyl-CoA from the cytoplasmic pool toward nuclear-localized ERG13 may create an optimal flux balance, minimizing metabolic interference from competing cytosolic pathways (Wang & Li, 2017).

The rational, bioinformatics-guided redesign of HMG1 further illustrates the necessity of empirical validation in metabolic engineering. Initially, we identified variant 522tHMG1 by TMHMM (Moller et al., 2001), which modestly improved α -santalene yields, prompting exploration of previously characterized variants (531tHMG1 (Polakowski et al., 1998) and AA531tHMG1 (Donald et al., 1997)). The dramatically differing catalytic performances of these closely related variants indicate the impact of subtle structural variations, likely influencing protein stability, catalytic kinetics, or other post-transcriptional processes, emphasizing the necessity for careful enzyme design in metabolic engineering. In particular, the superior activity of 531tHMG1 compared to AA531tHMG1 and 522tHMG1 warrants further investigation to

elucidate the underlying mechanisms.

We further demonstrated the value of genomic context engineering in metabolic pathway optimization. By integrating IDI1/ERG13 (or ERG13-NES) and ERG20/ERG10 (or ERG10-NES) expression cassettes at the DPP1 and LPP1 loci, respectively, we not only achieved high-level overexpression of key pathway enzymes but also disrupted the activity of diacylglycerol pyrophosphate phosphatase. This dual effect reduced unwanted FPP hydrolysis and channeled more precursor toward α -santalene biosynthesis. The observed improvements in production likely reflect the combined effects of ERG13 relocalization, IDI1 co-overexpression, and DPP1 disruption. Although not all single-variable controls were constructed in this study, future work systematically dissecting the contributions of each genetic modification will be crucial for clarifying their individual impacts on pathway flux and product yield.

Importantly, overexpression of ERG20 and ERG10 alone did not enhance α -santalene titers, likely because the increased FPP pool was continued to be consumed by native sterol biosynthesis via ERG9. This indicates the need for coordinated regulation of both precursor supply and downstream metabolic flux. Only after replacing the native ERG9 promoter with the weak, glucose-inducible pHXT1 promoter (Lewis & Bisson, 1991) was FPP efficiently redirected into the target pathway, emphasizing the critical role of critical flux control at multiple pathway nodes. While our data support the notion that ERG20 overexpression without ERG9 downregulation leads to greater flux toward sterol biosynthesis, we did not directly quantify squalene or sterol intermediates. Future studies involving targeted metabolite profiling will be essential to validate flux redistribution and further elucidate the metabolic effects of these engineering strategies.

Medium optimization further enhanced production titers, with 2.5 mM betaine supplementation proving particularly effective, likely due to enhanced cellular resilience to fermentation stresses (Thomas et al., 1994). Betaine is a well- characterized osmoprotectant in yeast and other microorganisms, functioning to stabilize proteins and membranes and maintain osmotic balance under stressful conditions (Kang et al., 2012; Thomas et al., 1994). This enhanced stress tolerance may improve yeast viability and metabolic activity during fermentation, especially in the presence of hydrophobic products like α-santalene, which can otherwise disrupt membrane integrity. Thus, betaine supplementation likely supports higher product yields by mitigating toxicity and maintaining cellular homeostasis. Finally, the scalability and robustness of our engineered strain were validated by achieving an industrially competitive titer of 568.59 mg/L in 5-L fed-batch fermentation, positioning this strain among the highest reported producers of α -santalene in yeast systems.

Overall, this work demonstrates that a modular metabolic engineering strategy, combining spatial enzyme rewiring, target genes overexpression, promoter engineering, and process optimization, can achieve robust and scalable sesquiterpene biosynthesis. These results establish enzyme subcellular localization engineering and chromosomal context design as powerful, generalizable tools for advancing yeast metabolic engineering.

While our current focus was on overcoming spatial and expression bottlenecks to achieve high $\alpha\text{-santalene}$ titers, additional strategies could further enhance pathway performance. Future work may include expanding precursor and cofactor pools (e.g., acetyl-CoA, NADPH), improving redox and energy balance, optimizing intracellular trafficking and efflux of hydrophobic products, or implementing dynamic control circuits. These strategies are currently under active exploration in our laboratory, with the aim of creating a more versatile and high-performing yeast chassis for sesquiterpene and related natural product biosynthesis.

5. Conclusions

This study exemplifies how rational subcellular localization engineering, coupled with pathway rewiring and genomic context

optimization, can unlock new levels of metabolic performance in eukaryotic cell factories. By systematically analyzing and strategically manipulating both the spatial organization of key enzymes and the genomic loci for overexpression, we resolved intrinsic pathway bottlenecks and revealed non-intuitive principles underlying optimal flux distribution. The integration of chromosomal engineering at LPP1 and DPP1, targeted promoter replacement at ERG9, and adaptive fermentation strategies not only enabled one of the highest reported α-santalene titer in S. cerevisiae to date (92 mg/L (Scalcinati et al., 2012b), 163 mg/L (Tippmann et al., 2016b), and approximately 197 mg/L (Zha et al., 2022)), but also established a broadly applicable framework for the efficient and sustainable production of high-value natural products. As advanced tools for programmable protein localization, synthetic compartment design, and dynamic metabolic control continue to emerge, spatial engineering will play an increasingly central role in next-generation synthetic biology and industrial biotechnology.

CRediT authorship contribution statement

Wenwen Tan: Writing – original draft, Visualization, Validation, Methodology, Formal analysis, Data curation. Shengkun Tong: Methodology, Formal analysis, Data curation. Yaojie Gao: Methodology, Formal analysis. Jing Wang: Data curation. Jingyu Zhang: Formal analysis. Zhiping Xie: Resources, Methodology. Huanqin Dai: Methodology, Data curation. Yu Liang: Data curation. Gao-Yi Tan: Methodology. Lixin Zhang: Writing – review & editing, Project administration, Funding acquisition, Conceptualization. Yaojun Tong: Writing – review & editing, Writing – original draft, Supervision, Project administration, Investigation, Funding acquisition, Conceptualization.

Declaration of competing interest

The authors declare that they have no known competing financial interests or personal relationships that could have appeared to influence the work reported in this paper.

Acknowledgements

This work was supported by grants from the National Key Research and Development Program of China (2021YFA0909500, 2020YFA0907200, and 2020YFA0907800), the National Natural Science Foundation of China (32170080, 32370026, and 32121005), Shanghai Pilot Program for Basic Research-Shanghai Jiao Tong University (21TQ1400204), Science and Technology Commission of Shanghai Municipality (24HC2810200). Open Funding Project of the State Key Laboratory of Microbial Metabolism (MMLKF22-03), and the 111 Project (B18022).

Appendix A. Supplementary data

Supplementary data to this article can be found online at https://doi.org/10.1016/j.biortech.2025.133027.

Data availability

Data will be made available on request.

References

Adams, D.R., Bhatnagar, S.P., Cookson, R.C., 1975. Sesquiterpenes of Santalum album and Santalum spicatum. Phytochemistry 14 (5), 1459–1460.

Avalos, J.L., Fink, G.R., Stephanopoulos, G., 2013. Compartmentalization of metabolic pathways in yeast mitochondria improves the production of branched-chain alcohols. Nat. Biotechnol. 31 (4), 335–341.

Awan, A.R., Blount, B.A., Bell, D.J., Shaw, W.M., Ho, J.C.H., McKiernan, R.M., Ellis, T., 2017. Biosynthesis of the antibiotic nonribosomal peptide penicillin in baker's yeast. Nat. Commun. 8 (1), 15202.

- Bommareddy, A., Brozena, S., Steigerwalt, J., Landis, T., Hughes, S., Mabry, E., Knopp, A., VanWert, A.L., Dwivedi, C., 2019. Medicinal properties of alpha-santalol, a naturally occurring constituent of sandalwood oil: review. Nat. Prod. Res. 33 (4), 527–543
- Bröker, J.N., Müller, B., van Deenen, N., Prüfer, D., Schulze Gronover, C., 2018. Upregulating the mevalonate pathway and repressing sterol synthesis in *Saccharomyces cerevisiae* enhances the production of triterpenes. Appl. Microbiol. Biotechnol. 102 (16), 6923–6934.
- Burdock, G.A., Carabin, L.G., 2008. Safety assessment of sandalwood oil (Santalum album L.). Food Chem. Toxicol. 46 (2), 421–432.
- Celedon, J.M., Chiang, A., Yuen, M.M.S., Diaz-Chavez, M.L., Madilao, L.L., Finnegan, P. M., Barbour, E.L., Bohlmann, J., 2016. Heartwood-specific transcriptome and metabolite signatures of tropical sandalwood (*Santalum album*) reveal the final step of (Z)-santalol fragrance biosynthesis. Plant J. 86 (4), 289–299.
- Chen, R., Wang, M., Keasling, J.D., Hu, T., Yin, X., 2024. Expanding the structural diversity of terpenes by synthetic biology approaches. Trends Biotechnol. 42 (6), 699–713.
- DiCarlo, J.E., Norville, J.E., Mali, P., Rios, X., Aach, J., Church, G.M., 2013. Genome engineering in *Saccharomyces cerevisiae* using CRISPR-Cas systems. Nucleic Acids Res. 41 (7), 4336–4343.
- Donald, K.A., Hampton, R.Y., Fritz, I.B., 1997. Effects of overproduction of the catalytic domain of 3-hydroxy-3-methylglutaryl coenzyme A reductase on squalene synthesis in Saccharomyces cerevisiae. Appl. Environ. Microbiol. 63 (9), 3341–3344.
- Engler, C., Kandzia, R., Marillonnet, S., 2008. A one pot, one step, precision cloning method with high throughput capability. PLoS One 3 (11), e3647.
- Gadal, O., Strauss, D., Kessl, J., Trumpower, B., Tollervey, D., Hurt, E., 2001. Nuclear export of 60S ribosomal subunits depends on Xpo1p and requires a nuclear export sequence-containing factor, Nmd3p, that associates with the large subunit protein Rpl10p. Mol. Cell Biol. 21 (10), 3405–3415.
- Geraldi, A., Khairunnisa, F., Farah, N., Bui, L.M., Rahman, Z., 2021. Synthetic scaffold systems for increasing the efficiency of metabolic pathways in microorganisms. Biology 10 (3), 216.
- Gibson, D.G., 2011. Enzymatic assembly of overlapping DNA fragments. Methods Enzymol. 498, 349–361.
- Gietz, R.D., Schiestl, R.H., 2007. High-efficiency yeast transformation using the LiAc/SS carrier DNA/PEG method. Nat. Protoc. 2 (1), 31–34.
- Grewal, P.S., Samson, J.A., Baker, J.J., Choi, B., Dueber, J.E., 2021. Peroxisome compartmentalization of a toxic enzyme improves alkaloid production. Nat. Chem. Biol. 17 (1), 96–103.
- Hong, K.K., Nielsen, J., 2012. Metabolic engineering of Saccharomyces cerevisiae: a key cell factory platform for future biorefineries. Cell. Mol. Life Sci. 69 (16), 2671–2690.Kang, W.Y., Kim, S.H., Chae, Y.K., 2012. Stress adaptation of Saccharomyces cerevisiae as
- Rang, W.Y., Kim, S.H., Chae, Y.K., 2012. Stress adaptation of Saccharomyces cereviside as monitored via metabolites using two-dimensional NMR spectroscopy. FEMS Yeast Res. 12 (5), 608–616.
- Kim, G.B., Kim, H., Lee, S.Y., 2025. Comprehensive evaluation of the capacities of microbial cell factories. Nat. Commun. 16, 2869.
- Kulagina, N., Besseau, S., Papon, N., Courdavault, V., 2021. Peroxisomes: A New Hub for Metabolic Engineering in Yeast. Front. Bioeng. Biotechnol. 7 (9), 659431.
- Lewis, D.A., Bisson, L.F., 1991. The *HXT1* gene product of *Saccharomyces cerevisiae* is a new member of the family of hexose transporters. Mol. Cell. Biol. 11 (7), 3804–3813.
- Liu, Y., Zhao, X., Gan, F., Chen, X., Deng, K., Crowe, S.A., Hudson, G.A., Belcher, M.S.,
 Schmidt, M., Astolfi, M.C.T., Kosina, S.M., Pang, B., Shao, M., Yin, J.,
 Sirirungruang, S., Iavarone, A.T., Reed, J., Martin, L.B.B., El-Demerdash, A.,
 Kikuchi, S., Misra, R.C., Liang, X., Cronce, M.J., Chen, X., Zhan, C., Kakumanu, R.,
 Baidoo, E.E.K., Chen, Y., Petzold, C.J., Northen, T.R., Osbourn, A., Scheller, H.,
 Keasling, J.D., 2024. Complete biosynthesis of QS-21 in engineered yeast. Nature
 629 (8013), 937–944.
- Livak, K.J., Schmittgen, T.D., 2001. Analysis of relative gene expression data using realtime quantitative PCR and the 2(-Delta Delta C(T)) Method. Methods 25 (4), 402-408
- Meng, X., Liu, H., Xu, W., Zhang, W., Wang, Z., Liu, W., 2020. Metabolic engineering Saccharomyces cerevisiae for de novo production of the sesquiterpenoid (+)nootkatone. Microb. Cell Fact. 19 (1), 21.
- Moller, S., Croning, M.D., Apweiler, R., 2001. Evaluation of methods for the prediction of membrane spanning regions. Bioinformatics 17 (7), 646–653.
- Ostergaard, S., Olsson, L., Nielsen, J., 2000. Metabolic engineering of Saccharomyces cerevisiae. Microbiol. Mol. Biol. Rev. 64 (1), 34–50.

- Polakowski, T., Stahl, U., Lang, C., 1998. Overexpression of a cytosolic hydroxymethylglutaryl-CoA reductase leads to squalene accumulation in yeast. Appl. Microbiol. Biotechnol. 49 (1), 66–71.
- Rothstein, R., 1991. Targeting, disruption, replacement, and allele rescue: integrative DNA transformation in yeast. In: Methods in Enzymology, 194. Academic Press, pp. 281–301.
- Scalcinati, G., Knuf, C., Partow, S., Chen, Y., Maury, J., Schalk, M., Daviet, L., Nielsen, J., Siewers, V., 2012. Dynamic control of gene expression in Saccharomyces cerevisiae engineered for the production of plant sesquitepene alpha-santalene in a fed-batch mode. Metab. Eng. 14 (2), 91–103.
- Scalcinati, G., Partow, S., Siewers, V., Schalk, M., Daviet, L., Nielsen, J., 2012c. Combined metabolic engineering of precursor and co-factor supply to increase α-santalene production by Saccharomyces cerevisiae. Microb. Cell Fact. 11, 117.
- Hallgren, J., Tsirigos, K.D., Pedersen, M.D., Almagro Armenteros, J.J., Marcatili, P., Nielsen, H., Krogh, A., Winther, O. 2022. DeepTMHMM predicts alpha and beta transmembrane proteins using deep neural networks. bioRxiv, 2022.04.08.487609.
- Schalk, M., 2013. Method for producing alpha-santalene:EP2252691. FIRMENICH & CIE. Schneider, C.A., Rasband, W.S., Eliceiri, K.W., 2012. NIH image to ImageJ: 25 years of image analysis. Nat. Methods 9 (7), 671–675.
- Song, S.Y., Ye, C.F., Jin, Y.J., Dai, H.X., Hu, J.P., Lian, J.Z., Pan, R.H., 2024. Peroxisome-based metabolic engineering for biomanufacturing and agriculture. Trends Biotechnol. 42 (9), 1161–1176.
- Thomas, K.C., Hynes, S.H., Ingledew, W.M., 1994. Effects of particulate materials and osmoprotectants on very-high-gravity ethanolic fermentation by *Saccharomyces cerevisiae*. Appl. Environ. Microbiol. 60 (5), 1519–1524.
- Tippmann, S., Scalcinati, G., Siewers, V., Nielsen, J., 2016. Production of farnesene and santalene by *Saccharomyces cerevisiae* using fed-batch cultivations with RQcontrolled feed. Biotechnol. Bioeng, 113 (1), 72–81.
- Voigt, C.A., 2020. Synthetic biology 2020-2030: six commercially-available products that are changing our world. Nat. Commun. 11, 6379.
- Wang, Y., Gong, X., Li, F., Zuo, S., Li, M., Zhao, J., Han, X., Wen, M., 2021. Optimized biosynthesis of santalenes and santalols in *Saccharomyces cerevisiae*. Appl. Microbiol. Biotechnol. 105 (23), 8795–8804.
- Wang, Y., Li, C., 2017. Metabolite transport and process enhancement in cell factories. Scientia Sinica Vitae 47 (5), 544–553.
- Yan, X.G., David, S.D., Du, G.Z., Li, W.G., Liang, D.M., Nie, S.X., Ge, M.Y., Wang, C., Qiao, J.J., Li, Y.N., Caiyin, Q., 2024. Biological properties of sandalwood oil and microbial synthesis of its major sesquiterpenoids. Biomolecules 14 (8), 971.
- Ye, C., Hong, H., Gao, J., Li, M., Gou, Y., Gao, D., Dong, C., Huang, L., Xu, Z., Lian, J., 2024. Characterization and engineering of peroxisome targeting sequences for compartmentalization engineering in *Pichia pastoris*. Biotechnol. Bioeng. 121 (7), 2091–2105.
- Zha, W.L., An, T.Y., Li, T., Zhu, J.X., Gao, K., Sun, Z.J., Xu, W.D., Lin, P.C., Zi, J.C., 2020. Reconstruction of the biosynthetic pathway of santalols under control of the GAL regulatory system in yeast. ACS Synth. Biol. 9 (2), 449–456.
- Zha, W.L., Zhang, F., Shao, J.Q., Ma, X.M., Zhu, J.X., Sun, P.H., Wu, R.B., Zi, J.C., 2022. Rationally engineering santalene synthase to readjust the component ratio of sandalwood oil. Nat. Commun. 13, 2508.
- Zhang, J., Hansen, L.G., Gudich, O., Viehrig, K., Lassen, L.M.M., Schrübbers, L., Adhikari, K.B., Rubaszka, P., Carrasquer-Alvarez, E., Chen, L., D'Ambrosio, V., Lehka, B., Haidar, A.K., Nallapareddy, S., Giannakou, K., Laloux, M., Arsovska, D., Jorgensen, M.A.K., Chan, L.J.G., Kristensen, M., Christensen, H.B., Sudarsan, S., Stander, E.A., Baidoo, E., Petzold, C.J., Wulff, T., O'Connor, S.E., Courdavault, V., Jensen, M.K., Keasling, J.D., 2022. A microbial supply chain for production of the anti-cancer drug vinblastine. Nature 609 (7926), 341–347.
- Zhang, Y., Yan, H., Niu, M., Cheng, Q., Zhang, X., Teixeira da Silva, J.A., Ma, G., 2017. Multiple strategies for increasing yields of essential oil and obtaining sandalwood terpenoids by biotechnological methods in sandalwood. Trees 32 (1), 17–28.
- Zhang, Y.M., Su, M., Chen, Y., Wang, Z., Nielsen, J., Liu, Z.H., 2023. Engineering yeast mitochondrial metabolism for 3-hydroxypropionate production. Biotechnol. Biofuel. Bioprod. 16, 64.
- Zhu, J., Zhang, Z.T., Tang, S.W., Zhao, B.S., Li, H., Song, J.Z., Li, D., Xie, Z., 2019. A validated set of fluorescent-protein-based markers for major organelles in yeast (Saccharomyces cerevisiae). MBio 10 (5), e01691–19.
- Zuo, Y.M., Xiao, F., Gao, J.C., Ye, C.F., Jiang, L.H., Dong, C., Lian, J.Z., 2022. Establishing Komagataella phaffii as a cell factory for efficient production of sesquiterpenoid alpha-santalene. J. Agric. Food Chem. 70 (26), 8024–8031.